

# Fibre-specific white matter changes in multiple sclerosis patients with optic neuritis



Sanuji Gajamange<sup>a</sup>, David Raffelt<sup>b</sup>, Thijs Dhollander<sup>b</sup>, Elaine Lui<sup>c</sup>, Anneke van der Walt<sup>d</sup>, Trevor Kilpatrick<sup>a</sup>, Joanne Fielding<sup>e</sup>, Alan Connelly<sup>b,f</sup>, Scott Kolbe<sup>a,b,\*</sup>

<sup>a</sup> Department of Anatomy and Neuroscience, University of Melbourne, Australia

<sup>b</sup> The Florey Institute of Neuroscience and Mental Health, Melbourne, Australia

<sup>c</sup> Department of Radiology, Royal Melbourne Hospital, University of Melbourne, Australia

<sup>d</sup> Department of Medicine, University of Melbourne, Australia

<sup>e</sup> School of Psychological Sciences, Monash University, Australia

<sup>f</sup> The Florey Department of Neuroscience and Mental Health, University of Melbourne, Australia

## ARTICLE INFO

### Keywords:

Multiple sclerosis

MRI

Diffusion

Optic neuritis

Axonal degeneration

Apparent fibre density

## ABSTRACT

Long term irreversible disability in multiple sclerosis (MS) is thought to be primarily driven by axonal degeneration. Axonal degeneration leads to degenerative atrophy, therefore early markers of axonal degeneration are required to predict clinical disability and treatment efficacy. Given that additional pathologies such as inflammation, demyelination and oedema are also present in MS, it is essential to develop axonal markers that are not confounded by these processes. The present study investigated a novel method for measuring axonal degeneration in MS based on high angular resolution diffusion magnetic resonance imaging. Unlike standard methods, this novel method involved advanced acquisition and modelling for improved axonal sensitivity and specificity. Recent work has developed analytical methods, two novel axonal markers, fibre density and cross-section, that can be estimated for each fibre direction in each voxel (termed a “fixel”). This technique, termed fixel-based analysis, thus simultaneously estimates axonal density and white matter atrophy from specific white matter tracts. Diffusion-weighted imaging datasets were acquired for 17 patients with a history of acute unilateral optic neuritis ( $35.3 \pm 10.2$  years, 11 females) and 14 healthy controls ( $32.7 \pm 4.8$  years, 8 females) on a 3 T scanner. Fibre density values were compared to standard diffusion tensor imaging parameters (fractional anisotropy and mean diffusivity) in lesions and normal appearing white matter. Group comparisons were performed for each fixel to assess putative differences in fibre density and fibre cross-section. Fibre density was observed to have a comparable sensitivity to fractional anisotropy for detecting white matter pathology in MS, but was not affected by crossing axonal fibres. Whole brain fixel-based analysis revealed significant reductions in fibre density and fibre cross-section in the inferior fronto-occipital fasciculus (including the optic radiations) of patients compared to controls. We interpret this result to indicate that this fixel-based approach is able to detect early loss of fibre density and cross-section in the optic radiations in MS patients with a history of optic neuritis. Fibre-specific markers of axonal degeneration should be investigated further for use in early stage therapeutic trials, or to monitor axonal injury in early stage MS.

## 1. Introduction

Multiple sclerosis (MS) is the most common neurological disorder affecting young adults. Pathologically, MS is characterised by the presence of inflammatory demyelinating lesions, associated with axonal loss within the central nervous system. Axonal degeneration leads to neurodegeneration visible as atrophy that is known to be associated

with clinical disability (De Stefano et al., 2014). Therefore, early markers that are indicative of atrophy are required to predict clinical disability.

In acute MS lesions, inflammatory cells can directly injure axons leading to axonal transection and subsequently Wallerian and retrograde degeneration (Trapp and Stys, 2009). Additionally, chronic demyelination can lead to axonal degeneration via excitotoxic

**Abbreviations:** MS, multiple sclerosis; FD, fibre density; FC, fibre cross-section; FDC, fibre density and cross-section; SS3T-CSD, single-shell 3-tissue constrained spherical deconvolution; ILF, inferior longitudinal fasciculus

\* Corresponding author at: Melbourne Brain Centre, 30 Royal Pde, Parkville, VIC 3054, Australia.

E-mail address: [kolbes@unimelb.edu.au](mailto:kolbes@unimelb.edu.au) (S. Kolbe).

<http://dx.doi.org/10.1016/j.nicl.2017.09.027>

Received 29 June 2017; Received in revised form 13 September 2017; Accepted 27 September 2017

Available online 29 September 2017

2213-1582/ © 2017 Published by Elsevier Inc. This is an open access article under the CC BY-NC-ND license (<http://creativecommons.org/licenses/by-nc-nd/4.0/>).

mechanisms due to the reliance on excess sodium channels required to transmit action potentials along denuded axonal segments (Trapp and Stys, 2009). Trans-synaptic degeneration can also occur due to loss of synaptic inputs from degenerating afferent neurons (Ghetti et al., 1972; Cook and Wisniewski, 1987; Ginsberg and Martin, 2002) or loss of efferent targets (Reich et al., 2009). With therapeutic interventions and clinical trials aiming to reduce or reverse axonal degeneration, there is a need for quantitative in vivo markers that can quantify axonal degeneration specifically and sensitively in early stage MS.

Diffusion weighted MRI, a technique that is sensitive to diffusion of water molecules, can provide information about the underlying microstructure of the brain. Diffusion tensor imaging, a method introduced over 20 years ago (Basser et al., 1994), remains the standard approach for quantifying diffusion in clinical neuroimaging studies. Voxel based metrics derived from diffusion tensor imaging include fractional anisotropy, reflecting the degree of diffusion anisotropy, and mean diffusivity, reflecting the overall magnitude of diffusion. Cross-sectional diffusion tensor imaging studies in MS patients have repeatedly reported reduced fractional anisotropy and increased mean diffusivity within lesions and normal appearing white matter (Ciccarelli et al., 2001; Gratsias et al., 2015). However, diffusion tensor imaging only models diffusion assuming a model of Gaussian diffusion for a single population of parallel axons, and is thus confounded by partial volume effects in voxels containing multiple fibre populations (up to 90% of white matter voxels), CSF and other non-axonal cell types (Alexander et al., 2001; Metzler-Baddeley et al., 2012; Jeurissen et al., 2013).

More recently, methods combining high angular resolution and higher diffusion weighting with higher-order diffusion models have been developed to overcome limitations of diffusion tensor imaging (Tuch et al., 2003; Tournier et al., 2004; Assaf and Basser, 2005; Wedeen et al., 2005; Wang et al., 2011; Raffelt et al., 2012b; Zhang et al., 2012; Dell'Acqua et al., 2013). However, some of these diffusion models suffer limitations including: (1) the estimation of diffusion distributions (Tuch et al., 2003; Wedeen et al., 2005) rather than fibre distributions that are better able to delineate crossing fibres of  $< 90^\circ$  separation (Tournier et al., 2008), or (2) estimation of diffusion parameters averaged over whole voxels without considering each fibre population separately (Wang et al., 2011; Zhang et al., 2012).

Here we utilize a diffusion analysis method that seeks to overcome these limitations, broadly termed “Fixel Based Analysis”. Using constrained spherical deconvolution, it is possible to estimate the continuous fibre orientation distribution for each voxel (Tournier et al., 2007). By segmenting the fibre orientation distributions within each voxel, individual underlying fibre populations (termed “fixels”) can be identified (Raffelt et al., 2017). Previous studies have shown that the fibre orientation distribution amplitude is proportional to the apparent fibre density of axons aligned in that direction (Raffelt et al., 2012b). Also, nonlinear registration of fibre orientation distributions provides information regarding local macroscopic volumetric changes in the white matter, termed fibre cross-section. Fixels can thus be used to represent fibre density and cross-section for each fibre population at a sub-voxel level for group-level statistical comparison (Raffelt et al., 2015). Fixel based analysis therefore allows for simultaneous group analysis of microscopic fibre density and macroscopic white matter tract atrophy across the entire white matter.

Ultimately fixel-based analyses could provide early markers of fibre specific axonal loss in MS for use in disease monitoring and prognosis. To that end, we first undertook a study aiming to examine pathological changes in FD in the white matter of people with MS, and the qualitative and quantitative relationships between FD and standard diffusion tensor imaging metrics. We then used whole brain fixel-based analysis to compare FD and FC between people with MS who presented with optic neuritis and healthy control subjects. We hypothesised that FD there would be reduced fibre density and cross-section in the primary visual pathway consistent with previous observations of microstructural

changes in this pathway in patients with optic neuritis (Kolbe et al., 2012a).

## 2. Methods

### 2.1. Subjects

Seventeen patients (age 21–50 years; 11 females, 6 males) with a history of optic neuritis (disease duration  $4.48 \pm 0.61$  years) were recruited from the Royal Victorian Eye and Ear Hospital, Australia. These patients were a subset of a cohort of patients ( $n = 38$ ) who were recruited to study optic pathway changes after acute optic neuritis (van der Walt et al., 2013). This subset agreed to return for a research MRI scanning session three and five years after initial recruitment to study longer term outcomes after optic neuritis. At the time of testing, all patients had been diagnosed with clinically definite MS according to the 2010 McDonald criteria and twelve out of seventeen patients were receiving treatment. All patients were experiencing acute optic neuritis at the time of recruitment and some patients also experienced subsequent relapses prior to scanning for this study. Fourteen healthy controls (age 27–43 years; 8 females, 6 males) with no reported history of neurological disease were recruited for comparisons. Disease severity was assessed in all patients with the Expanded Disability Status Scale (EDSS) (median: 1; range: 0–2).

This study was conducted in accordance with the Declaration of Helsinki and was approved by the Human Research Ethics Committees of the Royal Victorian Eye and Ear Hospital and the Royal Melbourne Hospital. All study participants provided voluntary, written consent.

### 2.2. Ocular testing

Optic nerve and retinal injury were measured using two techniques: (1) optical coherence tomography of the retina to measure the thickness of the retinal nerve fibre layer, and (2) multifocal visual evoked potential amplitude to measure loss of visual pathway conductance associated with axonal loss. Optical coherence tomography was performed using an OCT-3 scanner (Stratus™, software version 3.0, Carl Zeiss Meditec Inc.) using the Fast RNFL protocol. The acquisition consists of three circular 3.4 mm diameter scans centred on the optic disc. Scans with signal strength of  $< 7$  were discarded. Multifocal visual evoked potentials were recorded using the Accumap™ (Objectivision: Opera, Sydney, Australia) by a trained technician. The procedure entailed recording from 58 sectors of the visual field with four electrodes placed over theinion on the rear of the skull. Eyes were individually stimulated for 10 to 12 runs until a sufficient signal to noise ratio was reached.

### 2.3. MRI acquisition

Image acquisition was performed using a Siemens Trio 3 T MRI system (Siemens, Erlangen, Germany) with a 32 channel head coil. Diffusion weighted imaging (DWI) data were acquired with the following parameters: repetition time = 7800 ms, echo time = 112 ms, voxel size =  $2.5 \times 2.5 \times 2.5 \text{ mm}^3$ . Sixty diffusion-weighted images ( $b = 3000 \text{ s/mm}^2$ ), and seven non-diffusion weighted images ( $b = 0$ ) were acquired with a spin-echo echo planar imaging sequence. A pair of non-diffusion weighted images with opposite phase encoding was also acquired to correct for susceptibility induced distortion. In addition, T1-weighted MPRAGE images (repetition time = 1900, echo time = 2.63 ms; flip angle =  $9^\circ$ ; voxel size =  $0.8 \times 0.8 \times 0.8 \text{ mm}^3$ ) were acquired. Lastly, T2-weighted double inversion recovery SPACE images (repetition time = 7400 ms, effective echo time = 105 ms; inversion times = 3000 and 450 ms, echo train length = 194, flip angle =  $120^\circ$ ; voxel size =  $1.1 \times 1.1 \times 1.1 \text{ mm}^3$  sagittal acquisition) were obtained for patients to identify T2 hyperintense brain lesions. Lesions were segmented and verified by a neuroradiologist of nine years

experience (EL), who was blinded to each patient's clinical status using MRICro ([www.cabi.gatech.edu/mricro/mricro/](http://www.cabi.gatech.edu/mricro/mricro/)).

## 2.4. Diffusion imaging processing

### 2.4.1. Diffusion-weighted MRI pre-processing

Diffusion-weighted MRI pre-processing involved field-map correction of EPI distortions (TOPUP, FSL, v5.0.4), motion correction with correction for current-induced distortions (refer to Appendix A of Raffelt et al., 2012b), bias field correction (N4, <http://stnava.github.io/ANTs/>). Data was also intensity normalised across all subjects using the median  $b = 0 \text{ s/mm}^2$  intensity within a white matter mask and up-sampling by a factor of two to improve fibre orientation distribution registration and statistics (Raffelt et al., 2012b).

Diffusion tensor imaging analysis was performed with MRtrix3. Fractional anisotropy and mean diffusivity maps were derived for each subject. Note that voxels were masked out if the mean diffusivity values were deemed physically implausible (negative or 100 times greater than the median).

### 2.4.2. Fibre orientation distribution calculation

To generate a more accurate, specific and sensitive representation of the white matter fibre orientation distribution, single-shell 3-tissue constrained spherical deconvolution (SS3T-CSD) was applied using tissue-specific response functions for white matter, grey matter and cerebrospinal fluid (Dhollander and Connelly, 2016; Dhollander et al., 2016). These response functions are tissue-specific signal models, derived from the diffusion data itself. While subsequent analysis steps focus exclusively on fibre density measured from the white matter fibre orientation distributions, the inclusion of grey matter and cerebrospinal fluid components in the model accounts for the remainder of the complete diffusion-weighted MRI signal due to healthy tissues as well as contributions from certain inflammatory cells (Dhollander et al., 2017). Both response function estimation and SS3T-CSD are fully unsupervised and directly driven by the diffusion-weighted MRI data itself.

### 2.4.3. Fibre orientation distribution template construction

A population-averaged fibre orientation distribution template was generated from a subset of subjects (10 patients and 10 controls). In brief, the fibre orientation distribution of each subject was repeatedly non-linearly registered to optimise the template (Raffelt et al., 2011, 2012a). For each subject, a deformation field that encodes nonlinear transformations to the template space was generated. The fibre orientation distributions in the template are first segmented to identify fixels that are mapped reasonably well across all subjects in both populations—we will refer to this outcome as the fixel template analysis mask.

### 2.4.4. Fibre density and cross-section calculation

Firstly, each subject's fibre orientation distribution map was transformed to the fibre orientation distribution template and segmented to identify the subject fixels in each voxel. Secondly, the fixels were re-orientated and correspondences between the subject fixels and the template fixels were computed.

Fixel-specific measures are calculated for each fixel in the fixel template analysis mask. The integral of fibre orientation distribution lobes is proportional to the intra-axonal volume of axons oriented along the fixel direction, and can be interpreted as the apparent fibre density (Raffelt et al., 2012b, 2017). Unlike standard diffusion tensor imaging metrics, each individual fixel is associated with a specific fibre density (FD) metric, even in voxels that contain multiple fibre populations. Furthermore, the deformation field created from the registration of each fibre orientation distribution map to the template contains morphological information about cross-sectional volume changes of white matter fibre bundles. The Jacobian determinant of the deformation field

is able to quantify such local volumetric changes. Local expansion and contraction perpendicular to the fixel orientation provides a quantitative assessment of fibre cross-section (FC) differences (Raffelt et al., 2017). By multiplying fibre density and fibre cross-section at each fixel, a combined measure of fibre density and cross-section (FDC) is generated as well. The FDC accounts for both the microscopic and macroscopic changes in a fibre bundle.

**2.4.4.1. Comparisons between fibre density and diffusion tensor imaging in pathological white matter.** To evaluate fibre density against standard diffusion tensor imaging metrics, we performed qualitative regional and quantitative whole brain comparisons. These comparisons required us to convert fibre density from a fixel-wise measure to a simplified voxel-wise measure, and thus reduced the amount of potential information encoded in the fixel-based analysis. The angular integral of the fibre orientation distribution in each voxel was considered as the total fibre density.

For the qualitative analysis, we identified regions of interest in a single MS patient to evaluate fibre density in two lesions of differing severity and corresponding regions in a healthy control were also investigated. Firstly, the fibre orientation distribution maps were transformed into template space to allow for comparison between subjects. Voxel-wise measures, total fibre density and fractional anisotropy, were examined within the regions of interest ( $31 \times 31$  voxels), which included the lesion and surrounding white matter. To examine the non-linear difference between fractional anisotropy from total fibre density, a spatial representation of the difference between the two measures was calculated by subtracting the two measures after normalisation by their maximum and minimum values. Given that the scales for total fibre density and fractional anisotropy are different, normalisation provides values that are within the same scale. For all images, the maximum FD and FA voxels were not outliers (all data points are clearly presented in Fig. 1B scatterplots).

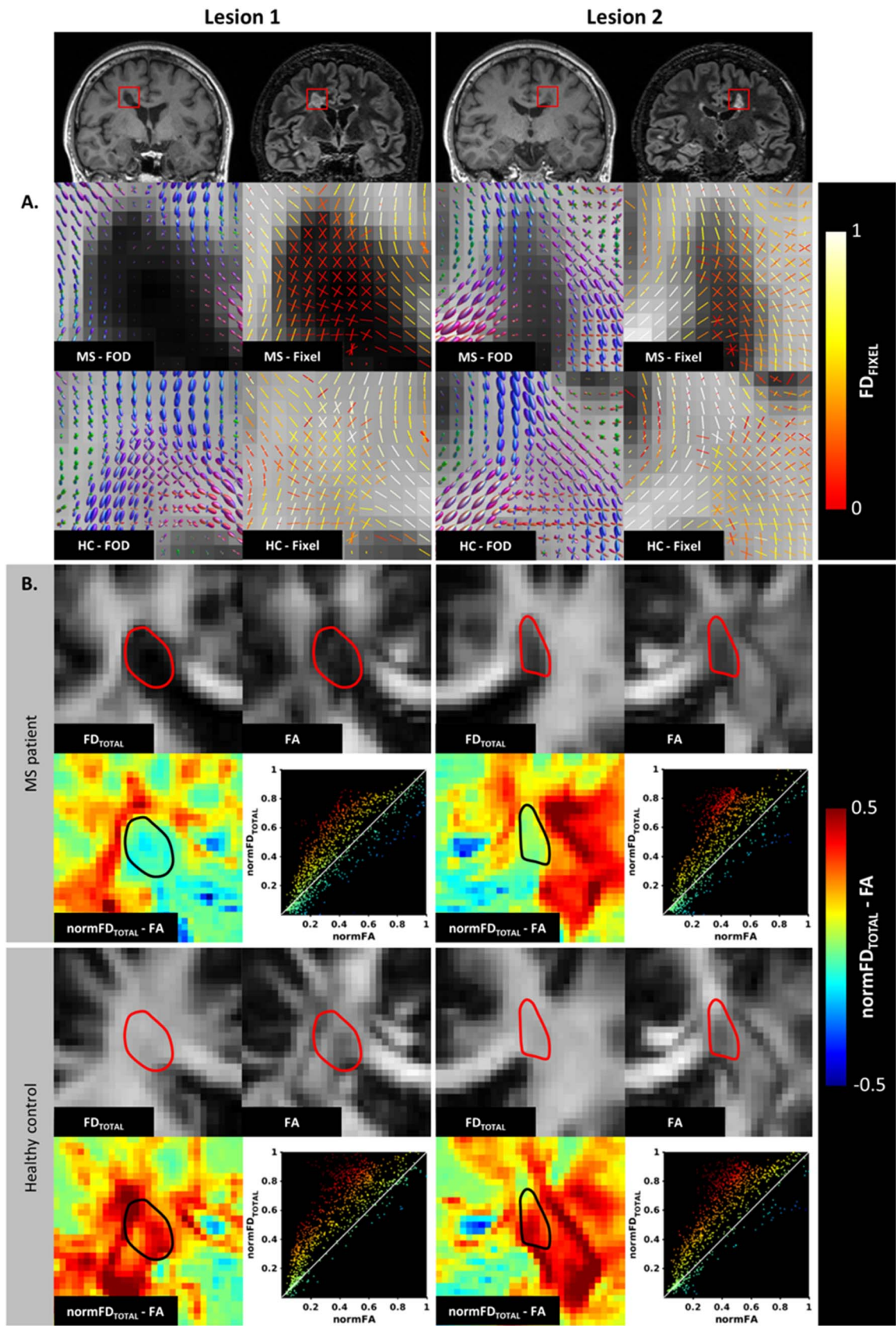
For the quantitative analysis, each subject's T1-weighted image was segmented to generate a binary white matter mask using MRtrix. A rigid affine registration (ANTs, version 1.5) was used to transform tissue masks to diffusion MRI space using nearest neighbour interpolation. In patients, binary lesion masks were registered from double inversion recovery image space to diffusion space with a rigid affine registration with a nearest neighbour interpolation. For patients, the lesion mask was subtracted from the white matter mask to create a normal appearing white matter mask.

**2.4.4.2. Whole-brain statistical analysis of fixel measures.** FD, FC and FDC were compared between groups using fixel-based analyses. Template-based probabilistic tractography (angle =  $22.5^\circ$ , maxlength = 250 mm, minlength = 10 mm, power = 1.0, tracks = 20 million) was performed to identify structurally connected fixels that are more likely to share underlying anatomy and pathology. Tractograms were filtered to minimise tractography seeding biases (Smith et al., 2013) using MRtrix. This process resulted in a final track count of 2 million that was used for connectivity-based smoothing and statistical inference. In short, the template-based tractography map was used to identify fixels that are anatomically connected given that each fibre tract can be pathologically affected differently.

**2.4.4.3. Correlations between fixel-wise measures and brain and ocular measures.** Post-hoc correlation analyses were performed between the fixel-wise measures and both brain volume and ocular measures in patients in order to better interpret the sources of pathological variance in fixel measures. Average FD and FC were obtained from regions of interest including all significant fixels identified using fixel-based analysis.

Measures of brain and optic nerve injury were calculated to correlate with fixel measures. From the optical coherence tomography the average retinal nerve fibre layer thickness was calculated for each eye. From





(caption on next page)

**Fig. 1.** Focal comparisons between fibre density and fractional anisotropy in lesions and healthy white matter. (A) Lesions of differing severity from a single MS patient and the corresponding region in a healthy control illustrates the pathological effects on fibre orientation distributions (FOD) and corresponding fixel fibre density (FD). In lesion 1 with severe axonal loss there is a complete loss of fibre density (no white matter fibre orientation distributions detected). There is also some evidence of disrupted fibre directions in the lateral perilesional white matter compared to the control subject. In lesion 2 there is a more moderate reduction of FOD amplitude and preservation of fibre directions compared to the healthy control. (B) Shows voxelwise comparisons between total fibre density and fractional anisotropy within the same two lesions and the surrounding white matter. The spatial maps showing the difference between normalised total fibre density and normalised fractional anisotropy show regions of large differences between fibre density and fractional anisotropy, particularly in regions of crossing fibres in the healthy white matter. The corresponding scatter plots (line through unity) further illustrate the differences between the measures.

multifocal visual evoked potential, the mean amplitude was calculated for each visual field sector and then for each eye as a whole. All measures from the affected eye were expressed as a normalised asymmetric percentage to account for inter-subject variation, while all measures from the unaffected eye were expressed as raw values. Brain volume measures were calculated with FreeSurfer (version 5.1.0) using the standard pipeline (Fischl et al., 2002) and expressed as fractions of intracranial volume to account for differences in head size. Specifically, lateral ventricle, cortical grey matter, subcortical grey matter (encompassing the thalamus, caudate, accumbens and ventral diencephalon) were examined.

## 2.5. Statistical analyses

### 2.5.1. Comparison between fibre density and diffusion tensor imaging

The average total fibre density, fractional anisotropy and mean diffusivity were extracted using the binary masks for each subject. A paired *t*-test was used to compare lesions to normal appearing white matter in patients, and independent sample *t*-tests were used to compare lesions and normal appearing patient white matter to healthy white matter in control subjects. Correction for multiple comparisons was performed with FDR.

### 2.5.2. Whole-brain fixel-based analysis

To compare quantitative measures at each fixel, general linear models were used to identify significantly reduced FD, FC and FDC for each fixel in patients compared to controls. Unlike voxel-based analysis, fixel-based analysis takes into consideration that a white matter voxel can contain multiple fibre populations, and each population can be independently affected by distal or proximal damage. Family-wise error corrected *p*-values were assigned to each fixel with nonparametric permutation testing using 5000 permutations (Raffelt et al., 2015). Significance was denoted by family-wise error corrected  $p < 0.05$ . To visualise the findings, the tractography map was cropped to include the streamlines that correspond with significant fixels.

### 2.5.3. Correlation between fixel-wise measures and, brain and ocular injury

Volumetric measures were compared between groups with independent samples *t*-tests (for equal and unequal variances) or Mann-Whitney *U* tests when violations of the assumption of normality occurred. Spearman correlation analyses were performed between regional fixel measures and structural and functional measures of visual and brain injury, after correcting for age as a covariate using linear regression. Correlations were considered significant at  $p < 0.05$ . Corrections for multiple comparisons were performed with FDR.

## 3. Results

Table 1 summarises demographic and disease related data for patients and control subjects. Patients exhibited extant loss of retinal nerve fibre layer thickness and visual evoked potential amplitude for the affected eye. Compared to controls, patients displayed significant atrophy of cortical grey matter but no ventricular enlargement, and cerebral white matter and subcortical grey matter atrophy.

### 3.1. Qualitative comparisons between total fibre density and diffusion tensor imaging metrics in pathological tissue

The fibre orientation distributions generated with SS3T-CSD were qualitatively assessed in two lesions of differing severity (Fig. 1A). Close

inspection of lesion 1 revealed reduced fibre orientation distribution amplitudes associated with reduced fixel FD compared to healthy white matter. Within lesion 2, the fibre orientation distribution amplitudes were reduced, yet the fibre orientations were preserved relative to the healthy control data.

Voxel-wise total fibre density and fractional anisotropy metrics were qualitatively compared within the regions of interest in the MS patient and healthy control (Fig. 1B). The difference between the two measures provides a spatial representation of the nonlinearities between the measures in pathological tissue and crossing-fibres. Overall, total fibre density appears more homogeneous than fractional anisotropy in lesions and surrounding white matter. Importantly, reduction in fractional anisotropy is not specific to regions of pathology, but can also be seen in healthy areas where fibre tracts cross, including within the periventricular regions that were lesion in the patient. Scatterplots showing the relationships between normalised total fibre density and fractional anisotropy provide further qualitative insights into the nonlinearities between the two measures. As expected, voxels that deviate the most from the line of unity lie within regions of crossing fibres.

### 3.2. Quantitative comparisons between total fibre density and diffusion tensor imaging metrics in pathological tissue

Averaged measures for total fibre density, fractional anisotropy and mean diffusivity were calculated for each subject to characterize the degree of difference in these measures in lesions and normal appearing white matter compared to normal healthy white matter (Fig. 2). Both total fibre density and fractional anisotropy were significantly different for the following comparisons: (1) lesions vs healthy white matter (total fibre density:  $d = 5.70$ ,  $p = 0.86 \times 10^{-12}$ , fractional anisotropy:  $d = 3.56$ ,  $p = 5.57 \times 10^{-9}$ ), (2) lesions vs normal appearing white matter (total fibre density:  $d = 4.32$ ,  $p = 0.61 \times 10^{-9}$ , fractional anisotropy:  $d = 3.08$ ,  $p = 0.29 \times 10^{-6}$ ), and (3) normal appearing vs healthy white matter (total fibre density:  $d = 0.88$ ,  $p = 0.026$ ; fractional anisotropy:  $d = 1.06$ ,  $p = 0.007$ ). For mean diffusivity, a difference was detected between lesions and healthy white matter ( $d = 6.05$ ,  $p = 3.86 \times 10^{-12}$ ) and normal appearing white matter ( $d = 5.68$ ,  $p = 13.78 \times 10^{-12}$ ), yet no difference was detected between healthy and normal appearing white matter ( $d = 0.73$ ,  $p = 0.061$ ).

### 3.3. Changes in fixel-specific measures after optic neuritis

Whole brain fixel-based analyses reported significant bilateral reduction of FD, FC, and FDC in the inferior longitudinal fasciculi (ILF), and reduction of FDC in the cingulum bundles in patients compared to controls (Fig. 3). Refer to Supplementary Fig. 1 for fixel-wise Cohen's *d* values.

Average fibre density within the significant regions of interest did not correlate with visual (retinal nerve fibre layer thickness or visual evoked potential amplitude) or brain volumetric measures (lateral ventricle, subcortical or cortical grey matter) (Supplementary Table 1). Loss of fibre density was moderately associated with enlargement of the lateral ventricles ( $\rho = -0.52$ ,  $p = 0.035$ ).

## 4. Discussion

This study aimed to investigate the use of fixel-specific measures

**Table 1**

Demographics and clinical data. Measures describing the visual and MRI volumetric changes in patients and controls. Measures from the affected eye reported as an asymmetric percentage, normalised to the unaffected eye. Measures from the unaffected eye reported as a raw value. \*A Mann-Whitney *U* test was performed. RNFL = retinal nerve fibre layer, mfVEP = multifocal visual evoked potential.

	MS patients (n = 17) 11 females	Healthy controls (n = 14) 8 females	p-Value
Age (years)	35.3 ± 10.2	32.7 ± 4.8	<i>p</i> = 0.390
Lesion volume (mm <sup>3</sup> )	2811.13	–	–
EDSS score (median; range)	1; 0–4	–	–
Number of relapses (median; range)	2; 1–4	–	–
Disease duration (years)	4.48 ± 0.61	–	–
Visual measures			
RNFL			
Affected eye (%)	–14.06 ± 12.94	–	–
Unaffected eye (μm)	97.87 ± 13.23	–	–
mfVEP amplitude			
Affected eye (%)	–9.22 ± 16.86	–	–
Unaffected eye (nV)	170.74 ± 35.98	–	–
Volumetric measures (× 10 <sup>–2</sup> )			
Lateral ventricle fraction*	1.11 ± 0.67	0.80 ± 0.26	<i>U</i> = 84.00, <i>p</i> = 0.173
Subcortical grey matter fraction*	2.08 ± 0.19	2.12 ± 0.14	<i>t</i> <sub>29</sub> = –0.66, <i>p</i> = 0.512
Cortical grey matter fraction	35.12 ± 4.21	39.74 ± 2.75	<i>t</i> <sub>27.73</sub> = –3.67, <i>p</i> = 0.001
White matter fraction	31.91 ± 2.73	31.55 ± 2.53	<i>t</i> <sub>29</sub> = 0.37, <i>p</i> = 0.712

(fibre density (FD), fibre cross-section (FC), and fibre density & cross-section (FDC)) as markers for axonal loss in the context of MS. Fixel-based analysis has previously been used to investigate axonal changes in motor neurone disease, temporal lobe epilepsy and pubertal development (Raffelt et al., 2012b; Genc et al., 2017; Raffelt et al., 2017; Vaughan et al., 2017). In MS, white matter pathologies additional to axonal loss can include inflammation, demyelination, oedema and gliosis. However, by focusing on the anisotropic white matter component of the diffusion MRI signal, fibre density measures are highly specific for axonal density changes. Additionally, fixel-based analysis quantifies macroscopic volume changes. Given that axonal degeneration leads to progressive atrophy, which has been associated with irreversible disability, an early precursor of atrophy may aid to predict clinical disability. Axonal degeneration is a potential early marker. Here we have applied a fixel-based analysis in a cohort of early MS patients with a history of acute optic neuritis and shown that indeed fixel-based loss was detected in the visual pathway as we hypothesised.

#### 4.1. Fibre density and fibre cross-section of the ILF is reduced in optic neuritis patients

Using fixel-based analysis we compared FD, FC and FDC in healthy participants to those in white matter of patients with historical optic neuritis. Consistent with our expectations, we observed a relatively specific loss of fibre density, and to a lesser extent fibre cross-section in patients within the ILF, a white matter tract that connects the occipital and temporal lobes. Anatomically it sits closely with the optic radiations posterior to the lateral geniculate nuclei. In addition, reduced FD was reported in the cingulum, an important fibre bundle involved in

communication between the frontal, temporal and parietal lobes. Previous studies have shown that anterograde trans-synaptic degeneration after optic neuritis is associated with atrophy to the lateral geniculate nucleus, axonal degeneration to the optic radiation and cortical thinning to the visual cortex (Evangelou et al., 2001; Rocca et al., 2013; von Glehn et al., 2014; Tur et al., 2016). Indeed, previous diffusion tensor imaging studies by our group have reported loss of axial diffusivity in the optic radiations of patients with optic neuritis (Kolbe et al., 2012a, 2016). Loss of axial diffusivity is difficult to interpret pathologically but has been observed in the context of acute axonal injury (Song et al., 2003; Wu et al., 2007; Zhang et al., 2009). In contrast to previous studies, we employed a diffusion-weighted MRI sequence with high diffusion weighting (*b*-value = 3000 s/mm<sup>2</sup>), which results in near complete attenuation of the signal from fast diffusing extracellular free-water and longitudinal axonal diffusion. Also, the relatively long echo time employed for diffusion imaging (112 ms) was such that the T2 from myelin water was fully decayed. In addition, SS3T-CSD can improve the specificity to the white matter intra-axonal space by removing signal contributions from certain isotropic diffusion components that could be associated with inflammatory cell infiltration. We therefore postulate that the observed findings in this cohort with a relatively short disease duration reflect a loss of fibre density in visual pathways as the initial manifestation of damage, which is then followed by a reduction in fibre bundle cross-section. Considering that fibre density and cross-section are derived from two separate sources of information (diffusion signal and nonlinear transformation field respectively), the multiplication of their effects as FDC provides a more comprehensive measure that characterises both microscopic and macroscopic fibre changes simultaneously (Raffelt et al., 2017).

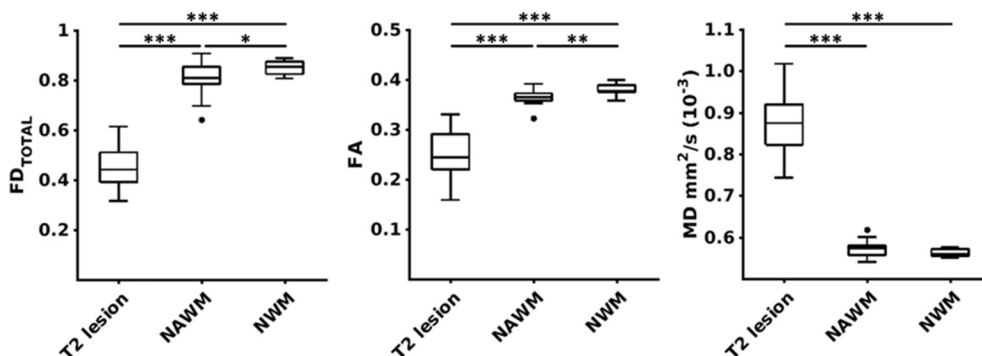


**Fig. 2.** Pathological effect size comparisons between fibre density and diffusion tensor imaging metrics. Subject-wise comparisons of average total fibre density (FD<sub>TOTAL</sub>), fractional anisotropy (FA) and mean diffusivity (MD) extracted from T2 lesions, normal appearing white matter (NAWM) and normal white matter (NWM) (\*\**p* = 0.001, \*\**p* = 0.01, \**p* = 0.05).



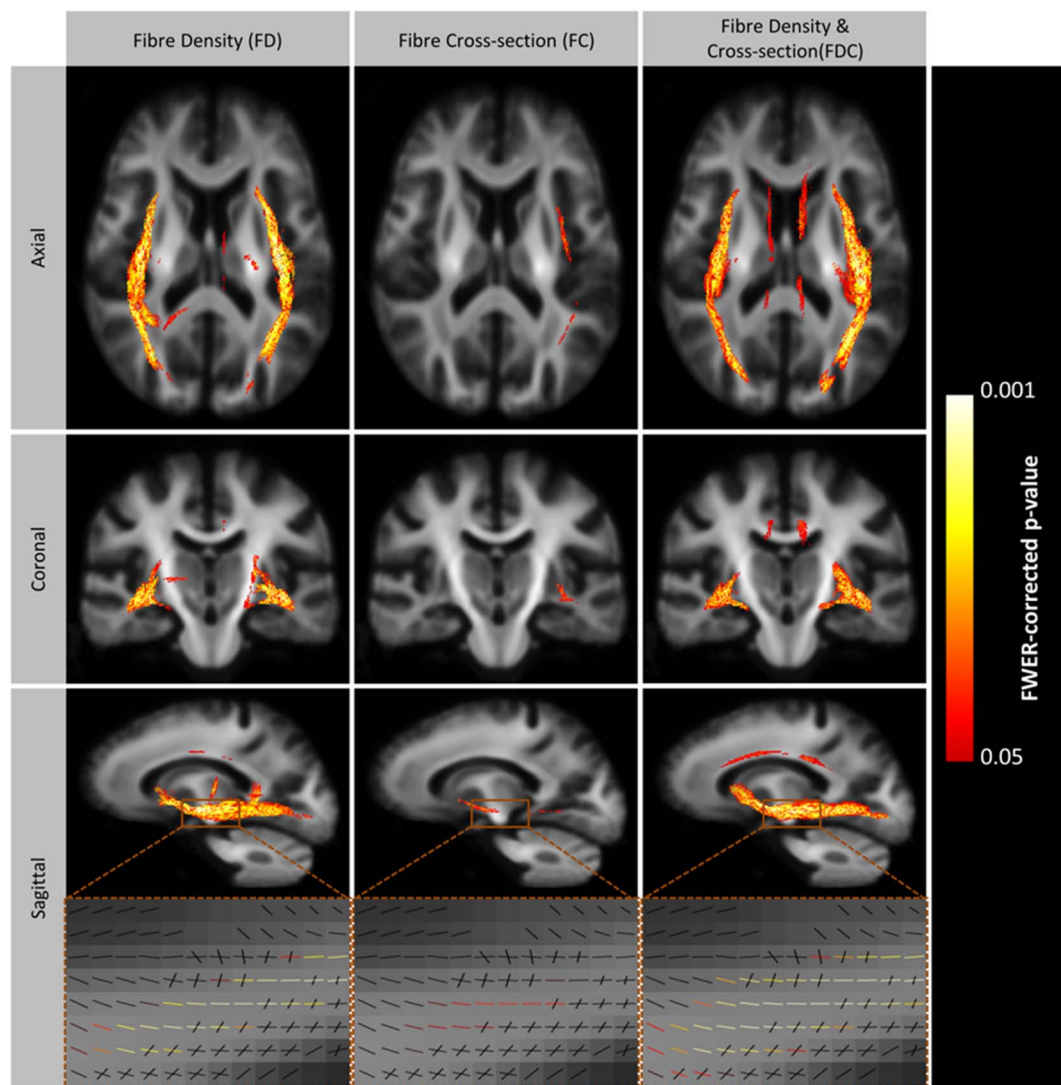


**Fig. 3.** Significant loss of fibre density, cross-section and fibre density and cross-section in the visual pathways of patients with a history of optic neuritis. To enable visualisation, streamlines from the template-derived whole-brain tractography map were cropped to include streamlines that correspond with significant fixels (family-wise error corrected  $p$ -value  $< 0.05$ ), and coloured by  $p$ -value. Significant tracts are overlaid on a 2D glass-brain in the axial, coronal and sagittal plane. A close-up of the significant fixels are displayed in the lowest panel. Results are displayed on the population-specific template. FD = fibre density, FC = fibre cross-section, FDC = fibre density and cross-section.

Contrary to our expectations, loss of optic radiation FDC was not correlated with the degree of optic nerve axonal loss or brain volume loss (apart from a trend with ventricular enlargement). We have previously shown that loss of optic radiation axial diffusivity correlated with affected optic nerve axonal loss measured using multifocal visual evoked potentials and optical coherence tomography (Kolbe et al., 2012b, 2016). Despite this apparent conflict, we are more confident in the current results given the greater pathological specificity of fibre density over diffusion tensor imaging markers such as axial diffusivity whose pathological substrate remains elusive. Also, the lack of correlation between fixel measures and grey matter atrophy further supports the notion that grey and white matter damage should be examined independently to provide a comprehensive assessment of neurodegeneration in people with MS.

#### 4.2. Diffusion metrics within lesions and normal appearing white matter

To better contextualise fibre density in terms of standard DTI parameters, we performed qualitatively and quantitative comparisons of lesions and NAWM. We observed a loss of fibre density in lesions and NAWM compared to healthy white matter. Focused assessments of

lesions demonstrated clear demarcation of lesion boundaries using FD. Despite the ability to identify lesions with fractional anisotropy, the metric exaggerates the loss of fibres due to crossing fibres and partial volume inclusion from other non-white matter tissue types, resulting in low fractional anisotropy. However, from the fibre orientation distribution and fixel overlays it is apparent that the lesions contain crossing fibres. Since some lesions have greater fibre loss than others, fibre density measures provide the opportunity to differentiate these lesions and their likely clinical consequences by using fixel-based analysis.

#### 4.3. Advantages of fixel-based analysis: diffusion model

Diffusion MRI sequences commonly used for diffusion tensor imaging employ low diffusion weighting ( $b$ -value  $\leq 1000$  s/mm<sup>2</sup>) which provides limited angular contrast and sensitivity to more rapidly moving molecular pools outside the axon. Furthermore, the diffusion tensor model does not account for the partial volume inclusion of other tissue types. Therefore, despite significant correlations reported between diffusion tensor imaging metrics and axonal density in post-mortem histology/imaging studies, diffusion tensor imaging parameters

are not solely affected by axonal density (Schmierer et al., 2007). Secondly, the diffusion tensor model assumes a single fibre orientation within each voxel; however, it is now known that ~90% of white matter voxels in the brain contain more than one fibre population (Jeurissen et al., 2013). Here, we overcome these limitations by estimating the complete fibre orientation distribution. In the context of MS, several other higher-order diffusion models have been proposed that can account for inflammation associated cellularity, gliosis and oedema (Assaf and Basser, 2005; Wang et al., 2011; Zhang et al., 2012). Similar to these methods, SS3T-CSD incorporates additional response functions for grey matter and CSF, which allow the partial volume fraction estimation of these signals in the white matter to improve the specificity to axonal contributions and damage (Dhollander and Connelly, 2016). It has been shown before that these “grey matter-like” and “CSF-like” signals can also account for signal contributions due to inflammatory processes, gliosis and oedema (Dhollander et al., 2017).

#### 4.4. Advantages of fixel-based analysis: statistical analysis

MS has increasingly been viewed as a disconnection syndrome with disruptions to white matter connectivity so a method for examining specific white matter tracts across multiple subjects is highly desirable (Rocca et al., 2015). The tract-based spatial statistics method has gained popularity in this context for the population analysis of diffusion tensor imaging data (Dineen et al., 2009; Roosendaal et al., 2009). Fixel-based analysis provides an alternative approach to statistically compare fixel-specific measures across subjects (Raffelt et al., 2015) by registering all image data to a common template (Raffelt et al., 2011, 2012a, 2017). Unlike voxel-based approaches, fixel-based analysis considers the connectivity between fixels in a directionally meaningful way such that signals from orthogonally intersecting tracts are not combined during statistical clustering. This is a critical innovation that recognises the fact that each fibre tract can be pathologically affected differently (Raffelt et al., 2015). Fixel connectivity is estimated by performing a template-based tractography to smooth and enhance fixels that are structurally connected. By doing so, fixel-based analysis can identify specific white matter tracts that exhibit a disruption to fibre connectivity allowing for more meaningful interpretation of white matter damage in terms of patient functional outcomes.

#### 4.5. Limitations and future work

In the current study we examined a relatively small clinically homogeneous sample of patients. However, the inclusion of patients with a consistent pathological insult (optic neuritis) provided a useful opportunity to examine the anatomical specificity of fixel-based analysis given the very specific hypothesis we were able to form regarding the location of axonal damage in the visual pathways. It should be noted that the current study included a cohort of early MS patients with minimum lesional damage, therefore there would not be a significant problem during the image registration steps. However, pathologically severe lesions that show complete loss of fibre density in the lesion core can potentially affect image registration locally. In future studies, we intend to examine more severe MS cases where the presence of lesions can be a problem during image registration. In addition, we aim to examine more heterogeneous and larger samples of patients over time to understand the temporal and spatial pattern of fixel-specific changes. Specifically, longitudinal studies will provide an opportunity to investigate the sensitivity of fixel measures for detecting changes in individual patients to provide effect size estimates for potential trials using fixel measures as endpoints. Additionally, the growing use of more realistic diffusion models to assess the underlying microstructure will require future research to compare these models in specific disease contexts. Finally, while we have inferred loss of fibre density to be associated with axonal loss based on solid theory, validation of the measure against gold standard histological measures of axonal density

would be advantageous for correctly interpreting fibre density changes in patients.

## 5. Conclusion

In summary, we have used fixel-based analysis to detect tract-specific loss of fibre density and cross-section in the posterior visual pathway following optic neuritis. We contend that the advantages provided by fixel-based analysis compared to conventional diffusion tensor methods (i.e. greater specificity for axonal density, sensitivity to damage in multiple fibre populations within a voxel, simultaneous measurement of microstructural and macroscopic neurodegenerative changes) have enabled improved understanding of the characteristics of white matter lesions and of more widespread white matter injury in MS. Importantly, this study has demonstrated that the fixel-based analysis as a potential early marker of clinical disability in MS. With advanced markers of axonal degeneration it can potentially aid in treatment efficacy and predict clinical outcome.

## Acknowledgements

This work was supported by the National Health and Medical Research Council (APP1009757, APP1054147), Multiple Sclerosis Research Australia (Postgraduate Scholarship #14-088, SG), the Victorian Life Sciences Computing Initiative (Resource Allocation Scheme #1529, SK). We would like to thank Dr. Annie Shelton for insightful comments on the manuscript, and the Murdoch Children's Research Institute MRI Centre for significant assistance with data collection.

## Appendix A. Supplementary data

Supplementary data to this article can be found online at <https://doi.org/10.1016/j.nicl.2017.09.027>.

## References

- Alexander, A.L., Hasan, K.M., Lazar, M., Tsuruda, J.S., Parker, D.L., 2001. Analysis of partial volume effects in diffusion-tensor MRI. *Magn. Reson. Med.* 45 (5), 770–780.
- Assaf, Y., Basser, P.J., 2005. Composite hindered and restricted model of diffusion (CHARMED) MR imaging of the human brain. *NeuroImage* 27 (1), 48–58.
- Basser, P.J., Mattiello, J., LeBihan, D.M.R., 1994. Diffusion tensor spectroscopy and imaging. *Biophys. J.* 66 (1), 259–267.
- Ciccarelli, O., Werring, D., Wheeler-Kingshott, C., Barker, G., Parker, G., Thompson, A., et al., 2001. Investigation of MS normal-appearing brain using diffusion tensor MRI with clinical correlations. *Neurology* 56 (7), 926–933.
- Cook, R.D., Wisniewski, H.M., 1987. The spatio-temporal pattern of Wallerian degeneration in the Rhesus monkey optic nerve. *Acta Neuropathol.* 72 (3), 261–267.
- De Stefano, N., Airas, L., Grigoriadis, N., Mattie, H.P., O'Riordan, J., Oreja-Guevara, C., et al., 2014. Clinical relevance of brain volume measures in multiple sclerosis. *CNS Drugs* 28 (2), 147–156.
- Dell'Acqua, F., Simmons, A., Williams, S.C., Catani, M., 2013. Can spherical deconvolution provide more information than fiber orientations? Hindrance modulated orientational anisotropy, a true-tract specific index to characterize white matter diffusion. *Hum. Brain Mapp.* 34 (10), 2464–2483.
- Dhollander, T., Connelly, A., 2016. A novel iterative approach to reap the benefits of multi-tissue CSD from just single-shell ( $b = 0$ ) diffusion MRI data. In: *Proceedings of the 24th Meeting of International Society for Magnetic Resonance in Medicine*, pp. 3010.
- Dhollander, T., Raffelt, D., Connelly, A., 2016. Unsupervised 3-tissue response function estimation from single-shell or multi-shell diffusion MR data without a co-registered T1 image. In: *Proceedings of the International Society for Magnetic Resonance in Medicine Workshop on Breaking the Barriers of Diffusion MRI*, pp. 5.
- Dhollander, T., Raffelt, D., Connelly, A., 2017. Towards interpretation of 3-tissue constrained spherical deconvolution results in pathology. In: *Proceedings of the 25th Meeting of International Society for Magnetic Resonance in Medicine*, pp. 1815.
- Dineen, R.A., Vilisaar, J., Hlinka, J., Bradshaw, C.M., Morgan, P.S., Constantinescu, C.S., et al., 2009. Disconnection as a mechanism for cognitive dysfunction in multiple sclerosis. *Brain* 132 (1), 239–249.
- Evangeliou, N., Konz, D., Esiri, M.M., Smith, S., Palace, J., Matthews, P.M., 2001. Size-selective neuronal changes in the anterior optic pathways suggest a differential susceptibility to injury in multiple sclerosis. *Brain* 124 (9), 1813–1820.
- Fischl, B., Salat, D.H., Busa, E., Albert, M., Dieterich, M., Haselgrove, C., et al., 2002. Whole brain segmentation: automated labeling of neuroanatomical structures in the



- human brain. *Neuron* 33 (3), 341–355.
- Genc, S., Seal, M.L., Dholander, T., Malpas, C.B., Hazell, P., Silk, T.J., 2017. White matter alterations at pubertal onset. *NeuroImage* 156, 286–292.
- Ghetti, B., Horoupian, D.S., Wisniewski, H.M., 1972. Transsynaptic response of the lateral geniculate nucleus and the pattern of degeneration of the nerve terminals in the Rhesus monkey after eye enucleation. *Brain Res.* 45 (1), 31–48.
- Ginsberg, S.D., Martin, L.J., 2002. Axonal transection in adult rat brain induces trans-synaptic apoptosis and persistent atrophy of target neurons. *J. Neurotrauma* 19 (1), 99–109.
- Gratsias, G., Kapsalaki, E., Kogia, S., Dardiotis, E., Tsimourtou, V., Lavdas, E., et al., 2015. A quantitative evaluation of damage in normal appearing white matter in patients with multiple sclerosis using diffusion tensor MR imaging at 3 T. *Acta Neurol. Belg.* 115 (2), 111–116.
- Jeurissen, B., Leemans, A., Tournier, J.-D., Jones, D.K., Sijbers, J., 2013. Investigating the prevalence of complex fiber configurations in white matter tissue with diffusion magnetic resonance imaging. *Hum. Brain Mapp.* 34 (11), 2747–2766.
- Kolbe, S., Bajraszewski, C., Chapman, C., Nguyen, T., Mitchell, P., Paine, M., et al., 2012a. Diffusion tensor imaging of the optic radiations after optic neuritis. *Hum. Brain Mapp.* 33 (9), 2047–2061.
- Kolbe, S., Marriott, M., van der Walt, A., Fielding, J., Klistorner, A., Mitchell, P.J., et al., 2012b. Diffusion tensor imaging correlates of visual impairment in multiple sclerosis and chronic optic neuritis. *Invest. Ophthalmol. Vis. Sci.* 53 (2), 825–832.
- Kolbe, S., van der Walt, A., Butzkueven, H., Klistorner, A., Egan, G.F., Kilpatrick, T.J., 2016. Serial diffusion tensor imaging of the optic radiations after acute optic neuritis. *J. Ophthalmol.* 2016, 6.
- Metzler-Baddeley, C., O'Sullivan, M.J., Bells, S., Pasternak, O., Jones, D.K., 2012. How and how not to correct for CSF-contamination in diffusion MRI. *NeuroImage* 59 (2), 1394–1403.
- Raffelt, D., Tournier, J.D., Fripp, J., Crozier, S., Connelly, A., Salvado, O., 2011. Symmetric diffeomorphic registration of fibre orientation distributions. *NeuroImage* 56 (3), 1171–1180.
- Raffelt, D., Tournier, J.D., Crozier, S., Connelly, A., Salvado, O., 2012a. Reorientation of fiber orientation distributions using apodized point spread functions. *Magn. Reson. Med.* 67 (3), 844–855.
- Raffelt, D., Tournier, J.D., Rose, S., Ridgway, G.R., Henderson, R., Crozier, S., et al., 2012b. Apparent fibre density: a novel measure for the analysis of diffusion-weighted magnetic resonance images. *NeuroImage* 59 (4), 3976–3994.
- Raffelt, D., Smith, R.E., Ridgway, G.R., Tournier, J.D., Vaughan, D.N., Rose, S., et al., 2015. Connectivity-based fixel enhancement: whole-brain statistical analysis of diffusion MRI measures in the presence of crossing fibres. *NeuroImage* 117, 40–55.
- Raffelt, D., Tournier, J.D., Smith, R.E., Vaughan, D.N., Jackson, G., Ridgway, G.R., et al., 2017. Investigating white matter fibre density and morphology using fixel-based analysis. *Neuroimage* 144 (Part A), 58–73.
- Reich, D.S., Smith, S.A., Gordon-Lipkin, E.M., Ozturk, A., Caffo, B.S., Balcer, L.J., et al., 2009. Damage to the optic radiation in multiple sclerosis is associated with retinal injury and visual disability. *Arch. Neurol.* 66 (8), 998–1006.
- Rocca, M.A., Mesaros, S., Preziosa, P., Pagani, E., Stolic-Opincal, T., Dujmovic-Basuroski, I., et al., 2013. Wallerian and trans-synaptic degeneration contribute to optic radiation damage in multiple sclerosis: a diffusion tensor MRI study. *Mult. Scler. J.* 19 (12), 1610–1617.
- Rocca, M.A., Amato, M.P., De Stefano, N., Enzinger, C., Geurts, J.J., Penner, I.-K., et al., 2015. Clinical and imaging assessment of cognitive dysfunction in multiple sclerosis. *Lancet Neurol.* 14 (3), 302–317.
- Roosendaal, S.D., Geurts, J.J.G., Vrenken, H., Hulst, H.E., Cover, K.S., Castelijns, J.A., et al., 2009. Regional DTI differences in multiple sclerosis patients. *NeuroImage* 44 (4), 1397–1403.
- Schmierer, K., Wheeler-Kingshott, C.A.M., Boulby, P.A., Scaravilli, F., Altmann, D.R., Barker, G.J., et al., 2007. Diffusion tensor imaging of post mortem multiple sclerosis brain. *NeuroImage* 35 (2), 467–477.
- Smith, R.E., Tournier, J.-D., Calamante, F., Connelly, A.S.I.F.T., 2013. Spherical-deconvolution informed filtering of tractograms. *NeuroImage* 67, 298–312.
- Song, S.-K., Sun, S.-W., W.-K. Ju, Lin, S.-J., Cross, A.H., Neufeld, A.H., 2003. Diffusion tensor imaging detects and differentiates axon and myelin degeneration in mouse optic nerve after retinal ischemia. *NeuroImage* 20 (3), 1714–1722.
- Tournier, J.D., Calamante, F., Gadian, D., Connelly, A., 2004. Direct estimation of the fiber orientation density function from diffusion-weighted MRI data using spherical deconvolution. *NeuroImage* 23 (3), 1176–1185.
- Tournier, J.D., Calamante, F., Connelly, A., 2007. Robust determination of the fibre orientation distribution in diffusion MRI: non-negativity constrained super-resolved spherical deconvolution. *NeuroImage* 35 (4), 1459–1472.
- Tournier, J.D., Yeh, C.-H., Calamante, F., Cho, K.-H., Connelly, A., Lin, C.-P., 2008. Resolving crossing fibres using constrained spherical deconvolution: validation using diffusion-weighted imaging phantom data. *NeuroImage* 42 (2), 617–625.
- Trapp, B.D., Stys, P.K., 2009. Virtual hypoxia and chronic necrosis of demyelinated axons in multiple sclerosis. *Lancet Neurol.* 8 (3), 280–291.
- Tuch, D.S., Reese, T.G., Wiegell, M.R., Van, J.W., 2003. Diffusion MRI of complex neural architecture. *Neuron* 40 (5), 885–895.
- Tur, C., Goodkin, O., Altmann, D.R., Jenkins, T.M., Miszkil, K., Mirigiani, A., et al., 2016. Longitudinal evidence for anterograde trans-synaptic degeneration after optic neuritis. *Brain* 139 (3), 816–828.
- van der Walt, A., Kolbe, S., Wang, Y., Klistorner, A., Shuey, N., Ahmadi, G., et al., 2013. Optic nerve diffusion tensor imaging after acute optic neuritis predicts axonal and visual outcomes. *PLoS One* 8 (12), e83825.
- Vaughan, D.N., Raffelt, D., Curwood, E., Tsai, M.-H., Tournier, J.-D., Connelly, A., et al., 2017. Tract-specific atrophy in focal epilepsy: disease, genetics, or seizures? *Ann. Neurol.* 81 (2), 240–250.
- von Glehn, F., Jarius, S., Cavalcanti Lira, R.P., Alves Ferreira, M.C., von Glehn, F.H.R., Costa e Castro, S.M., et al., 2014. Structural brain abnormalities are related to retinal nerve fiber layer thinning and disease duration in neuromyelitis optica spectrum disorders. *Mult. Scler. J.* 20 (9), 1189–1197.
- Wang, Y., Wang, Q., Haldar, J.P., Yeh, F.-C., Xie, M., Sun, P., et al., 2011. Quantification of increased cellularity during inflammatory demyelination. *Brain* 134 (12), 3587–3598.
- Wedeer, V.J., Hagmann, P., W.-YI, Tseng, Reese, T.G., Weisskoff, R.M., 2005. Mapping complex tissue architecture with diffusion spectrum magnetic resonance imaging. *Magn. Reson. Med.* 54 (6), 1377–1386.
- Wu, Q., Butzkueven, H., Gresle, M., Kirchhoff, F., Friedhuber, A., Yang, Q., et al., 2007. MR diffusion changes correlate with ultra-structurally defined axonal degeneration in murine optic nerve. *NeuroImage* 37 (4), 1138–1147.
- Zhang, J., Jones, M., DeBoy, C.A., Reich, D.S., Farrell, J.A.D., Hoffman, P.N., et al., 2009. Diffusion tensor magnetic resonance imaging of Wallerian degeneration in rat spinal cord after dorsal root axotomy. *J. Neurosci.* 29 (10), 3160–3171.
- Zhang, H., Schneider, T., Wheeler-Kingshott, C.A., Alexander, D.C.N.O.D.I., 2012. Practical in vivo neurite orientation dispersion and density imaging of the human brain. *NeuroImage* 61 (4), 1000–1016.